

Analytical Platform to Characterize Dopant Solution Concentrations, Charge Carrier Densities in Films and Interfaces, and Physical Diffusion in Polymers Utilizing Remote Field-Effect Transistors

Hyun-June Jang, Justine Wagner, Hui Li, Qingyang Zhang, Tushita Mukhopadhyaya, Howard E. Katz*

Department of Materials Science and Engineering, Johns Hopkins University, 3400 N. Charles St, Baltimore, USA

Key words: hole carrier quantification; doping; P3HT; F4TCNQ; conductive polymers; diffusion; FET

ABSTRACT: Characterizing doping effects in a conductive polymer and physical diffusion in a passive polymer were performed using a remote-gate field-effect transistor (RG FET) detection system that was able to measure the electrical potential perturbation of a polymer film coupled to the gate of a silicon FET. Poly(3-hexylthiophene) (P3HT) film doped using various concentrations of 2,3,5,6-tetrafluoro-7,7,8,8-tetracyanoquinodimethane (F4TCNQ) solutions imposed additional positive potentials on the P3HT RG, resulting in a lower threshold voltage (V_{th}) on the n-channel silicon FET. Changes in V_{th} were related to the induced hole concentrations and hole mobility in P3HT films by using our V_{th} shifting model for the RG FET. We discovered that the electron-donating P3HT and even inorganic materials, indium tin oxide and gold, showed similar electrical potential perturbations dependent on the concentration of F4TCNQ in overlying solutions as the dopant radical anions maximally covered the surfaces. This suggests that there are limited electroactive sites for F4TCNQ binding on electron donor surfaces which results in a similar number of positive charges in film materials forming dipoles with the F4TCNQ radical counteranions. The effect of electron acceptors such as 7,7,8,8-tetracyanoquinodimethane and tetracyanoethylene was compared with that of F4TCNQ in terms of V_{th} shift using our analytical tool, with differences attributed to acceptor size and reduction potential. Meanwhile, this FET analysis tool offered a means of monitoring the physical diffusion of small molecules, exemplified by F4TCNQ, in the passive polymer polystyrene, driven by concentration gradients. The technique allows for nondestructive, nonspectroscopic, ambient characterization of electron donor-acceptor interactions at surfaces.

Introduction

From the very first demonstration of dopant-induced conductivity in conjugated polymers¹, it has been recognized that conducting polymers would be crucial components of flexible and printable electronic devices²⁻⁴. While initial reports of conductive polymers have demonstrated promising electrical conductive values on the order of 1000 S/cm,⁵ the conductivity is limited due to the instability of dopants through degradation and volatilization⁶, dopant solubility⁷⁻⁹, and decreases in mobility resulting from the structural disruption through dopant incorporation¹⁰. Some of the highest recent polymer conductivities have been obtained by solution doping of already-deposited films, termed sequential solution doping, as opposed to solution blending of polymers and dopants before deposition¹¹⁻¹³. Sequential doping methods overcame issues of poor solubility of solute mixtures, produced more uniform morphology and are compatible with roll-to-roll solution processing. Therefore, it is of particular interest to characterize the sequential solution-doping process and quantify charge densities obtained from solution doping to best evaluate the usefulness of this process and possibly to obtain similar compositions and morphologies from solution depositions.

In organic electronics, it has been challenging to extract basic electrical parameters such as mobility and charge concentrations in doped polymers because of contributions from multiple variables^{2, 14}. Experimental conductivity (σ) and in-

nate carrier mobility (μ) from bulk inorganic materials allowed the calculation of carrier concentrations (p) using a classic relation in semiconductor physics, $\sigma = e\mu p$ where e is electron charge. In contrast, μ of organic films varies depending on morphologies and microstructures further influenced by doping concentrations and fabrication methods¹⁵⁻¹⁷. Specialized ways to calculate carrier concentrations such as capacitance-voltage¹⁸ and photoelectron spectroscopy¹⁹ were established but they require specially designed sample fabrication or complicated experimental setups.

Meanwhile, the diffusion of small molecules between organic layers provokes other serious issues in stability and lifetimes of organic electronics. The counter-ions formed from dopant molecules are free to drift under an electric field, either within films or into adjacent films, because they are not covalently bonded to the organic semiconductor²⁰. The diffusion of a relatively large p-dopant, 2,3,5,6-tetrafluoro-7,7,8,8-tetracyanoquinodimethane (F4TCNQ) over a layer consisting of either conjugated small molecules or polymer such as poly-3-hexylthiophene (P3HT) was investigated in recent work²⁰⁻²³. Despite these influences on electronic performance, they are rarely discussed because of limitations of current analysis tools. To be specific, monitoring diffusion using UV-Vis-NIR²¹ and photoluminescence (PL) spectroscopy²⁴ requires an observable interaction between host-materials and diffused molecules. It is even more challenging to measure simple

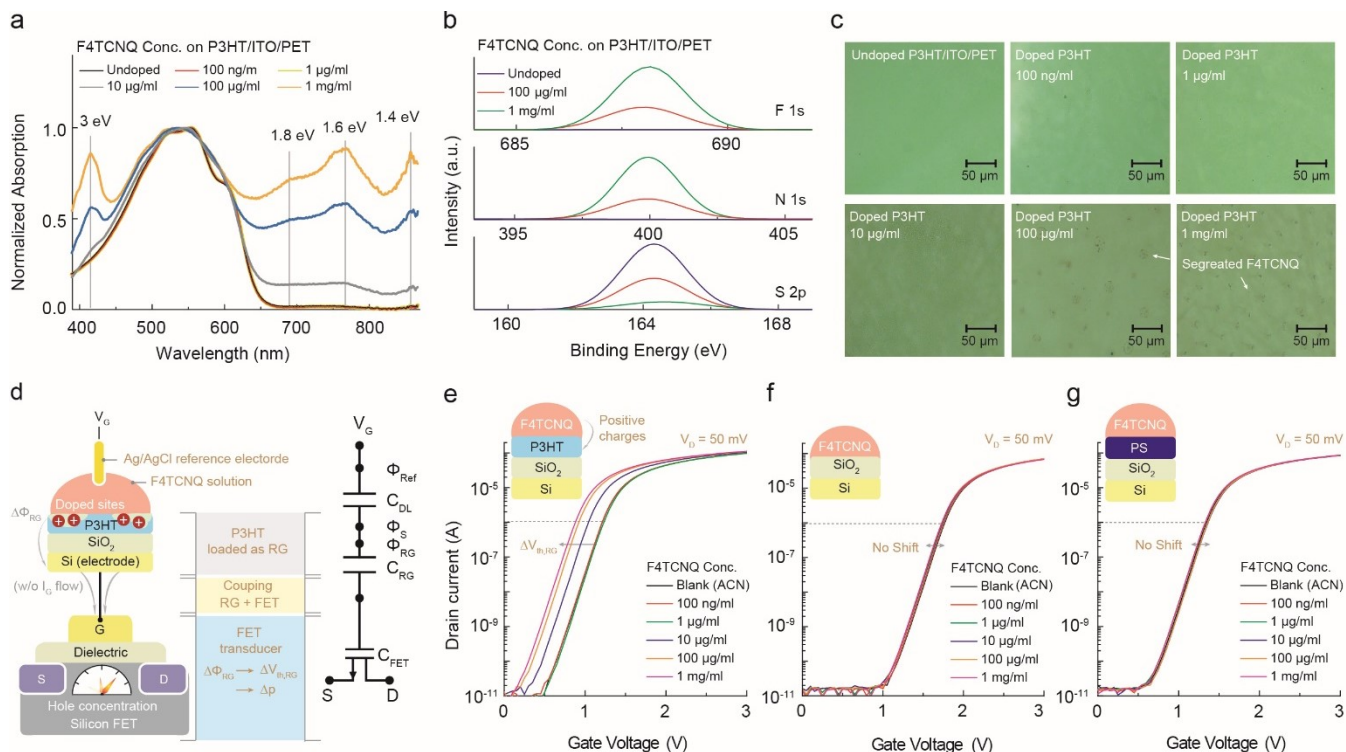


Figure 1. (a) UV-Vis-NIR spectra of P3HT films doped by F4TCNQ dissolved in ACN ranging from 100 ng/ml to 1 mg/ml. (b) XPS spectra and (c) microscopic images of the doped P3HT films processed identically to Figure 1(a). (d) Schematic image of RG FET system and equivalent circuit model for dopant quantification system. Response of transfer curves of RG FET with (e) P3HT/SiO₂, (f) SiO₂, and (g) PS/SiO₂ RGs for F4TCNQ solution concentrations.

physical diffusions of molecules through passive polymer dielectrics driven by concentration gradients and electric fields.

Herein, we developed a way to characterize doping effects and diffusion in polymers using a remote-gate (RG) FET setup which measures perturbations of the electrical potential of the polymer film on the RG coupled to the oxide gate of a silicon FET. The charge transfer between F4TCNQ and P3HT film doped via a sequential solution doping method on the RG was expressed as a shift in threshold voltage of the RG FET ($V_{th, RG}$). Using this setup, a new formula was established in order to calculate the induced hole concentrations in the doped P3HT film in terms of variation of $V_{th, RG}$ on the RG FET. F4TCNQ also reacted with the inorganic electron donor surfaces of gold (Au) and indium tin oxide (ITO) by making surface dipoles which resulted in the same $V_{th, RG}$ shift trend. In particular, we observed a similar range in electrical potentials of P3HT, Au, and ITO only regulated by concentrations of F4TCNQ as F4TCNQ fully occupied by the electroactive sites on those donor surfaces. The responsiveness of the other dopants such as 7,7,8,8-tetracyanoquinodimethane (TCNQ) and tetracyanoethylene (TCNE) related to their reduction potentials was observed using the RG FET system on both ITO and P3HT film. Meanwhile, signaling of F4TCNQ by ITO produced a new approach to monitor diffusion of small molecules through the passive, noninteraction polymer polystyrene (PS). F4TCNQ and ITO were used as a tracer and a sensing layer of the tracer, respectively. Thus, the dynamic doping of a conju-

gate polymer and transport of a dopant through an insulating polymer could both be observed and quantified on the remote FET gate.

Results and Discussion

Conventional spectroscopic observation of P3HT doping by F4TCNQ. Polaronic species, resulting from charge transfer between organic semiconductor and dopants, create many sub-gap absorptions that can be analyzed through UV-Vis-NIR spectroscopy²⁵. Figure 1(a) displays the UV-Vis-NIR spectra of P3HT films that are doped with varying F4TCNQ concentrations ranging from 100 ng/ml to 1 mg/ml in the solvent acetonitrile (ACN) that is orthogonal to the P3HT film. The spectra of the lightly doped P3HT films ($\leq 1 \mu\text{g/ml}$) are comparable to that of undoped P3HT film. Higher dopant concentration ($>1 \mu\text{g/ml}$) on P3HT began to produce distinct absorption bands at 3.0, 1.8, 1.6, and 1.4 eV resulting from the incorporation of F4TCNQ¹¹. The prominent 1.4 and 1.6 eV peaks described singly negatively charged F4TCNQ as F4TCNQ underwent integer charge transfers with P3HT sites²⁶. XPS spectra in Figure 1b showed F4TCNQ radical anions covering the surface of P3HT as an aggregate layer by revealing higher intensity signals of both F 1s and N 1s which originated from F4TCNQ and a less intense peak of S 2p, from P3HT. When the P3HT surface was fully dried after applying dopant solution, the microscopic images showed phase-segregated F4TCNQ domains (Figure 1c) due to the solubility limit of F4TCNQ in P3HT film (4.9 mol%) as reported¹¹.

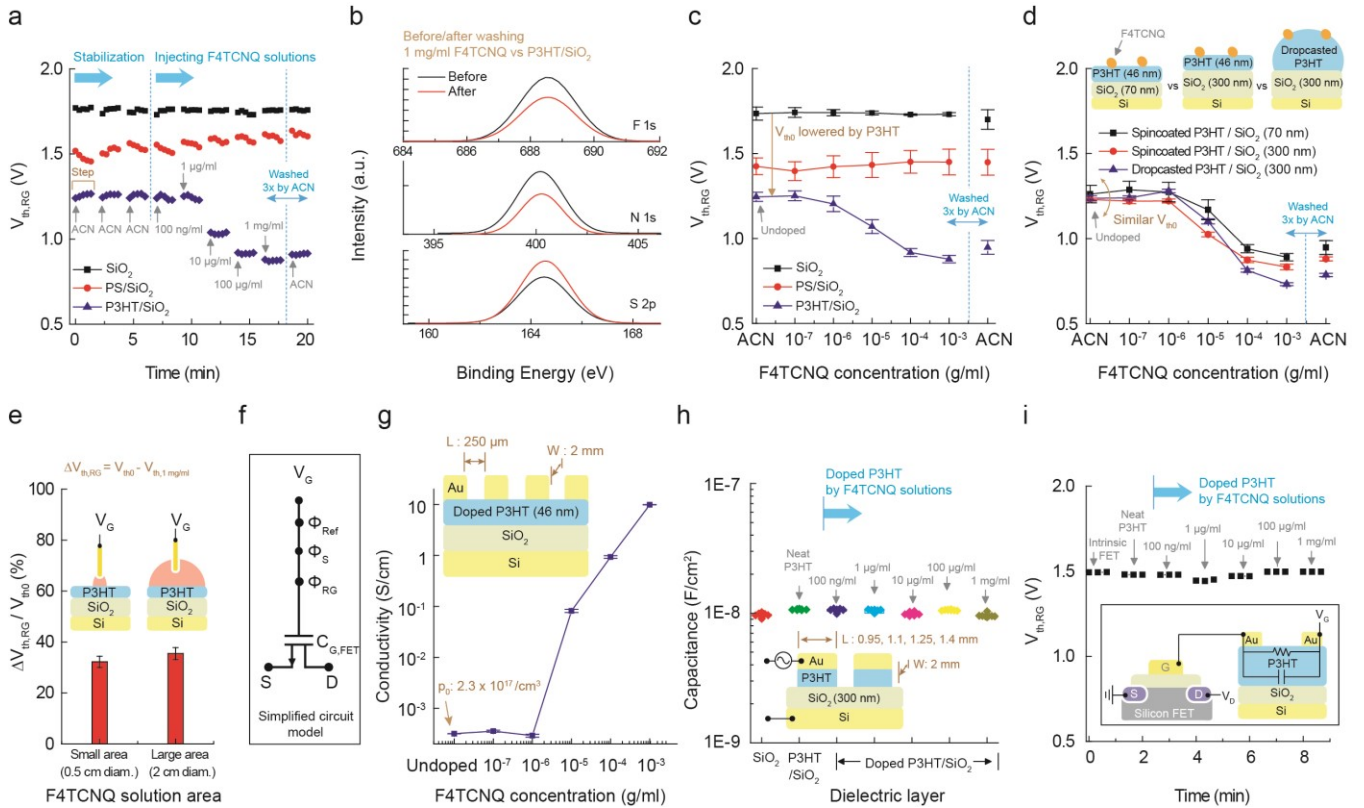


Figure 2. (a) Representative $V_{th,RG}$ response from P3HT/SiO₂, SiO₂, and PS/SiO₂ RG vs time for F4TCNQ solution concentrations. (b) XPS spectra of F 1s, N 1s, and S 2p from 1 mg/ml F4TCNQ:P3HT/SiO₂ before/after washing. (c) $V_{th,RG}$ distributions from P3HT/SiO₂, SiO₂, and PS/SiO₂ over at least 8 samples for F4TCNQ solution concentrations. (d) $V_{th,RG}$ distributions of RGs with spincoated P3HT on a 70-nm- and 300-nm-thick SiO₂ and dropcasted P3HT on a 300-nm-thick SiO₂ for F4TCNQ solution concentrations over at least 8 samples. (e) Distributions of $V_{th,RG}$ variation between $V_{th,1mg/ml}$ and V_{th0} of P3HT/SiO₂ RG measured under small (0.5 cm diameter) and large doping area (2 cm diameter) over at least 6 samples. (f) Simplified equivalent circuit model of RG FET system from Figure 1d. (g) Conductivity of doped P3HT measured by four-point probe over 4 samples. (h) Capacitance distributions of the doped P3HT/SiO₂ over 8 samples measured via metal-insulator-semiconductor structure. (i) $V_{th,RG}$ response of the doped P3HT film connected as an extra resistance or capacitance input to the gate of FET. Inset showed a schematic image in that electrical circuit.

RG doping assessments. Such doping effects were electrically analyzed via our RG FET detection system, which is demonstrated in Figure 1d. A P3HT film on a SiO₂/Si substrate was additionally coupled on the gate of a commercial silicon FET as a RG module by electrically connecting the RG to the gate of a silicon FET. An equivalent circuit model that included major components is shown in Figure 1d where C_{DL} , C_{RG} , and C_{FET} are capacitance of double-layer between solution and RG surface, RG material, and silicon FET, respectively. ϕ_{Ref} and ϕ_{RG} are work functions of reference electrode and RG material, and ϕ_S is the potential of the surface between the electrolyte and RG surface. Combining all capacitors in series and electrical potential from each material determined $V_{th,RG}$ of the RG FET system. For the main goal of quantifying hole carriers in the doped P3HT, a silicon FET measured variations in the electrical potential of the P3HT RG by mean of the $V_{th,RG}$ shift resulting from the generation of holes upon doping the surface of the P3HT film with varying concentrations of F4TCNQ in ACN (Figure 1d).

The reduced F4TCNQ on a P3HT RG triggered horizontal shifts in transfer curves of the RG FET by imposing positive charges on the RG (Figure 1e) relative to the solution potentials. During operation, there are no gate currents (\sim pA levels) through a P3HT RG (Figure S1). $V_{th,RG}$ shift was steadily saturated once the concentration reached 1 mg/ml F4TCNQ where the dopant fully covered the P3HT surface and made an aggregate layer as shown in Figure 1c. This overlaying F4TCNQ layer on the P3HT surface was shown in XPS depth profiling (Figure S2). The initial doped P3HT displayed higher concentrations of F4TCNQ on the surface and similar decreased amounts of dopants were observed from the shallow surface towards the gate oxide. In Figure 1f and 1g, no responses upon exposure to F4TCNQ were shown from two different control RGs which consisted of pure SiO₂/Si and PS/SiO₂/Si because no charge transfer occurred between SiO₂ and passive polymer PS layers and F4TCNQ, indicating no doping effects on SiO₂ and PS surfaces by F4TCNQ molecules.

Figure 2a shows the $V_{th,RG}$ responses from each RG for F4TCNQ concentrations over time. Each step includes 5 con-

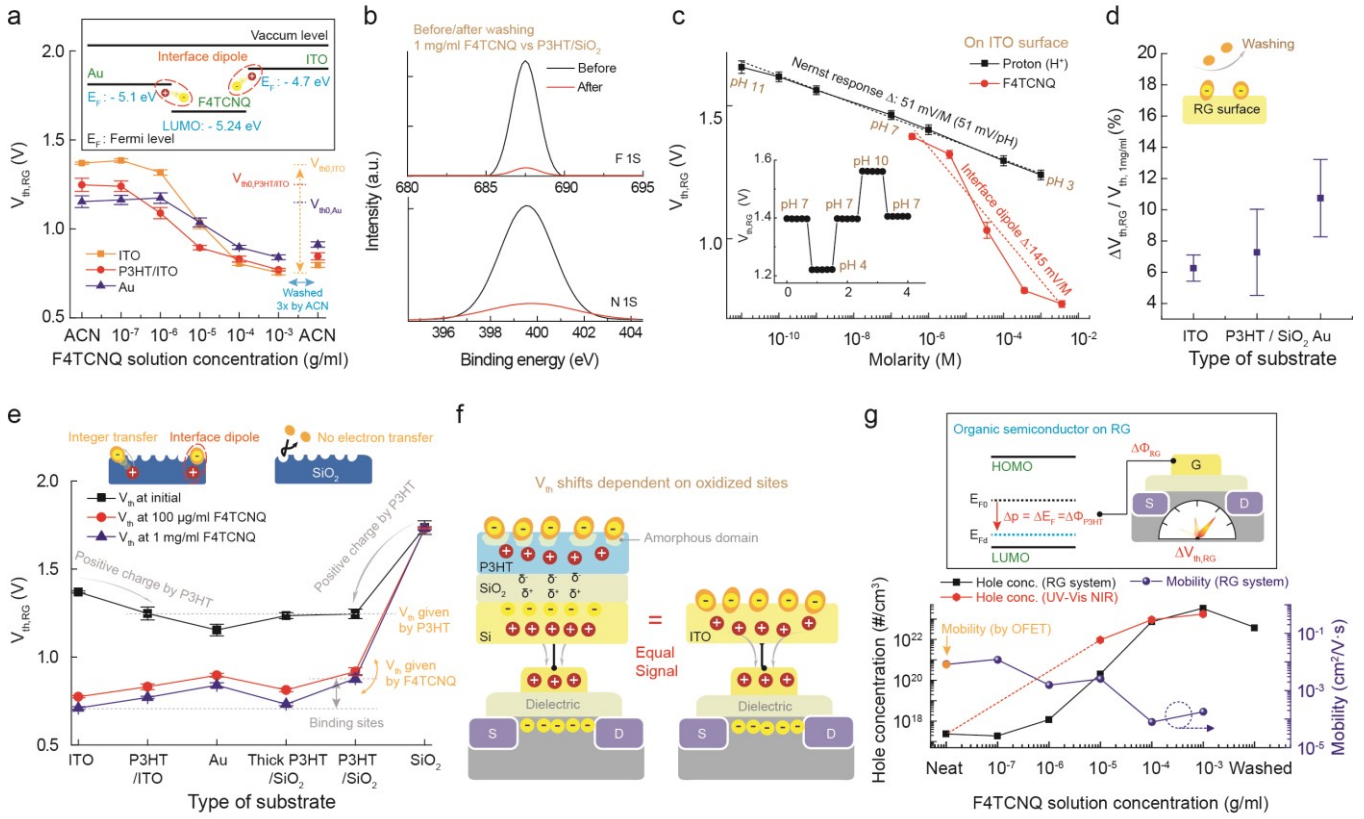


Figure 3. (a) $V_{th,RG}$ distributions over at least 8 samples vs. F4TCNQ concentrations on ITO, P3HT/ITO, and Au. Inset showed band diagram between Au or ITO and F4TCNQ. (b) XPS spectra regarding fluorine and nitrogen on 1 mg/ml F4TCNQ:ITO surface before/after washing. (c) Sensitivity to proton and F4TCNQ of ITO over at least 8 samples. Inset showed hysteresis curves in terms of changing concentration of proton (or pH). (d) Variation in $V_{th,RG}$ at 1 mg/ml F4TCNQ and neat ACN after washing with respect to each $V_{th,1mg/ml}$. (e) $V_{th,RG}$ distributions over at least 8 samples vs. type of RG substrate under the same solution condition of neat ACN, 100 $\mu\text{g/ml}$ F4TCNQ, and 1 mg/ml F4TCNQ. (f) Schematic image to describe $V_{th,RG}$ shift mechanism by occupation of F4TCNQ on electroactive sites on both P3HT and inorganic electron donors. (g) p_d calculated by $V_{th,RG}$ shifting model and UV-Vis NIR. Hole mobility calculated based on p_d from $V_{th,RG}$ shifting model. Inset showed schematic image of a concept to relate $\Delta V_{th,RG}$ to the induced p_d in P3HT.

secutive measurements taken at incremental times under a specific dopant concentration, demonstrated in Figure 2a. The first 3 steps were performed under pure ACN to measure initial $V_{th,RG}$ (V_{th0}) and stabilize our detection system. A sharp shift in $V_{th,RG}$ of P3HT exposed to F4TCNQ solutions higher than 1 $\mu\text{g/ml}$ showed that the doping process that was done sequentially was completed rapidly as reported in the literature¹¹. Following all the dopant injections, the doped P3HT was washed 3 consecutive times with pure ACN. Despite a slight increase of the resultant $V_{th,RG}$, there was no retrieval of the V_{th0} , indicating that doping reactions were mostly irreversible. Remaining F4TCNQ after washing was also observed by XPS (Figure 2b). Such $V_{th,RG}$ changes in terms of F4TCNQ concentrations were highly reproducible and uniform (Figure 2c) by revealing specific V_{th0} from each RG. Normalized variations of $V_{th,RG}$ with respect to V_{th0} showed a clear $V_{th,RG}$ window of P3HT for doping levels as offering the capability to quantitatively determine concentrations of dopant in that window (Figure S3).

We further investigated the mechanism in our detection system through following experiments. In the equivalent circuit model in Figure 1d, C_{FET} and Φ_{Ref} were invariable from the intrinsic silicon FET and Ag/AgCl reference electrode, respectively. As we only varied the concentration of F4TCNQ in ACN solution, ϕ_s that relied on proton concentrations was constant in the measurements. The influence of C_{DL} was insignificant in the total capacitance in the RG FET system because of the thinness of double layers, on the order of angstroms, and high dielectric constant of ACN²⁷⁻²⁸.

The effect of C_{RG} in $V_{th,RG}$ of the RG FET was estimated by changing thicknesses of both P3HT and SiO₂ dielectric of the RG (Figure 2d). A 46-nm-thick P3HT layer was spin coated on Si/SiO₂ substrates with different oxide thicknesses of 70 nm and 300 nm, respectively. Also, $V_{th,RG}$ responses of much thicker P3HT RGs made by drop-casting on a 300-nm-thick SiO₂ substrate was evaluated (Figure 2d and Figure S4). Despite these fabrication variables, all P3HT/SiO₂ RGs revealed a similar range in V_{th0} for the RG FET system (Figure 2d). This indicated that the fabrication variables in C_{RG} above were

insignificant compared to our large measured doping area of C_{RG} (0.5 cm diameter) which was used to make a contact with F4TCNQ solution on P3HT/SiO₂. Likewise, a larger doping area (2 cm diameter) led to a similar $V_{th,RG}$ shift (Figure 2e and Figure S5). Thus, the large measured area made the effect of C_{RG} negligible in relation to the total capacitance of RG FET as was case for the C_{DL} . Therefore, V_{th0} was given by the intrinsic property of P3HT and $V_{th,RG}$ shifts from V_{th0} reflecting the changed series voltage perturbation by P3HT as doped by F4TCNQ. However, very thick P3HT films produced more $V_{th,RG}$ shift for F4TCNQ over the solution concentration ranges, compared to spincoated P3HT (Figure S4b), resulting in the increase in number of electroactive sites per area than the spin-coated P3HT.

As a result, we can simplify an equivalent circuit model in Figure 1d by removing negligible parameters as shown in Figure 2f. The conventional definition of $V_{th,RG}$ of RG FET used for a pH sensor²⁹ can be modified by considering the electric potentials coming from intrinsic properties of RG material such as work function (Φ_{RG}) shown below:

$$V_{th,RG} = V_{th,FET} - \frac{\Phi_{Ref}}{q} - \frac{\Phi_{RG}}{q} + E_{Ref} - \chi^{Sol} - \Phi_S$$

where $V_{th,FET}$ is threshold voltage of silicon FET, χ^{Sol} is the electrolyte insulator surface dipole potential, and E_{Ref} is the potential of the reference electrode. $V_{th,FET}$ was fixed as 1.5 V (Figure S6) and Φ_{Ref} , E_{Ref} , Φ_S , and χ^{Sol} were consistent in our experimental setup. Therefore, the changes in $V_{th,RG}$ directly corresponded to a change in work function of RG material such as P3HT (Φ_{P3HT}):

$$\Delta V_{th,RG} = \Delta \Phi_{RG} = \Delta \Phi_{P3HT} \quad (1)$$

Subsequently, we measured conductivities (σ) of the doped P3HT films via four-point probe measurement (Figure 2g). Increasing conductivity of P3HT layer was shown from dopant concentration >1 $\mu\text{g/ml}$ F4TCNQ which corresponded to that of $V_{th,RG}$ shift in the RG FET setup (Figure 2c and Figure S3). A high conductivity of about 10 S/cm was realized from 1 mg/ml F4TCNQ. The initial hole concentration (p_0) was $2.4 \times 10^{17} \text{ cm}^{-3}$ calculated via $\sigma = e\mu_h p_0$ where σ of undoped P3HT was $3.2 \times 10^{-4} \text{ S/cm}$ (Figure 2g) and μ_h of $8.4 \times 10^{-3} \text{ cm}^2/\text{Vs}$ was calculated from making P3HT OFET (Figure S7). This μ_h value corresponded to that of $8.4 \times 10^{-3} \text{ cm}^2/\text{Vs}$ calculated via $\sigma = e\mu_h p_0$, which verified the calculated p_0 value. It is noted that a typical value of μ_h for spin-coated undoped P3HT is 0.01 cm^2/Vs in the literature³⁰. There were no distinct variations in capacitance of C_{RG} from doping reactions (Figure 2h), which also supported equation (1). The doped P3HT was connected as extra resistance and capacitance inputs on the RG (inset of Figure 2i) but no changes in $V_{th,RG}$ shift were observed (Figure 2i). This indicated that hole concentrations of doped P3HT (p_d) can be calculated using only terms of our $V_{th,RG}$ shift model independent of the conductivity of the films and based on the classic equation, $\sigma = e\mu_h p_0$.

Interestingly, pure ITO and Au surfaces showed a similar response to that of P3HT films with varying concentrations of F4TCNQ using the same measurement setup (Figure 3a). Rep-

resentative transfer curves and the $V_{th,RG}$ responses over time from Au and ITO for F4TCNQ concentrations are shown in Figure S8. This is explained as electron transfer from inorganic electrodes into F4TCNQ occurring when it was energetically favorable (inset of Figure 3a). The more negatively charged (oxyanionic) ITO surface was seen as a higher V_{th0} in the RG FET setup. ITO and P3HT being affected by the ITO³¹ responded to even lower concentration of F4TCNQ (1 $\mu\text{g/ml}$) via charge transfer. Saturated shifts in $V_{th,RG}$ upon increasing F4TCNQ concentrations were even shown with ITO and Au. That is, $V_{th,RG}$ was similarly saturated as surface dipole sites were fully occupied by F4TCNQ, as was the case for P3HT.

The restoration of $V_{th,RG}$ of ITO to the original value after washing off 1 mg/ml F4TCNQ solution using pure ACN was not observed, just as for the case of P3HT shown in Figure 2c. Despite adding four more washing steps for F4TCNQ:ITO, F4TCNQ still remained on the ITO, resulting from ionized F4TCNQ on the electron donor surfaces, either by doping or very strong intermolecular interactions, creating surface dipoles (Figure S9). This was more clearly shown in XPS spectra of the washed F4TCNQ:ITO surface by flowing the pure ACN for 5 sec (Figure 3b).

These responses from surface dipole sites can be compared with proton sensitivity by ITO³² showing $V_{th,RG}$ shift in terms of changes in Φ_S (Figure 3c) described with a site-binding model³³. The maximum sensitivity achievable in terms of a variable of concentration is 59 mV/pH at 25 °C, the well-known Nernst limit. ITO showed a linear response of 51 mV/M for every ten-fold increase in proton concentration and reversibly retrieved $V_{th,RG}$ for each pH value (inset of Figure 3c). Representative transfer curves regarding pH sensing are shown in Figure S10. ITO, however, showed nonlinear sensitivity to F4TCNQ measured to be 145 mV/M, beyond the Nernst limit, and irreversible $V_{th,RG}$ shifts. This may have indicated chemical reactions beyond simple coulomb attractions between F4TCNQ and ITO, or interactions on a rough ITO surface. Electrostatic strength of surface dipoles on each donor surface can be estimated by considering variation in $V_{th,RG}$ of ITO, Au, and P3HT at 1 mg/ml F4TCNQ ($V_{th,1\text{mg/ml}}$) and neat ACN after washing (Figure 3d) with respect to each $V_{th,1\text{mg/ml}}$. Au revealed a somewhat larger shift in $V_{th,RG}$ from washing effects, indicating weaker intermolecular interactions between F4TCNQ and Au surface. A larger difference between E_F of ITO and lowest unoccupied molecular orbital (LUMO) of F4TCNQ (inset of Figure 3a) may have contributed to stronger coulombic energy from dipoles.

$V_{th,RG}$ values were compared as a function of types of RG substrates under the same condition of each solution (Figure 3e). V_{th0} levels from each RG were uniform, respectively, and only depended on the type of materials. To be specific, P3HT showed a similar V_{th0} despite using different substrates such as SiO₂ and ITO. Likewise, F4TCNQ showed propensity that imposed specific $V_{th,RG}$ by interacting with each different RG (i.e. ~ 0.8 V at 1 mg/ml F4TCNQ). This behavior could be interpreted as a similar number density of F4TCNQ occupying and oxidizing the sites on each donor surface and the majority of F4TCNQ molecules underwent integer charge transfer with the electron donors²⁵. It also indicated constraints in oxidizing sites by F4TCNQ with any electron donor surface which led to a saturated $V_{th,RG}$ shift at high concentration of F4TCNQ (Fig-

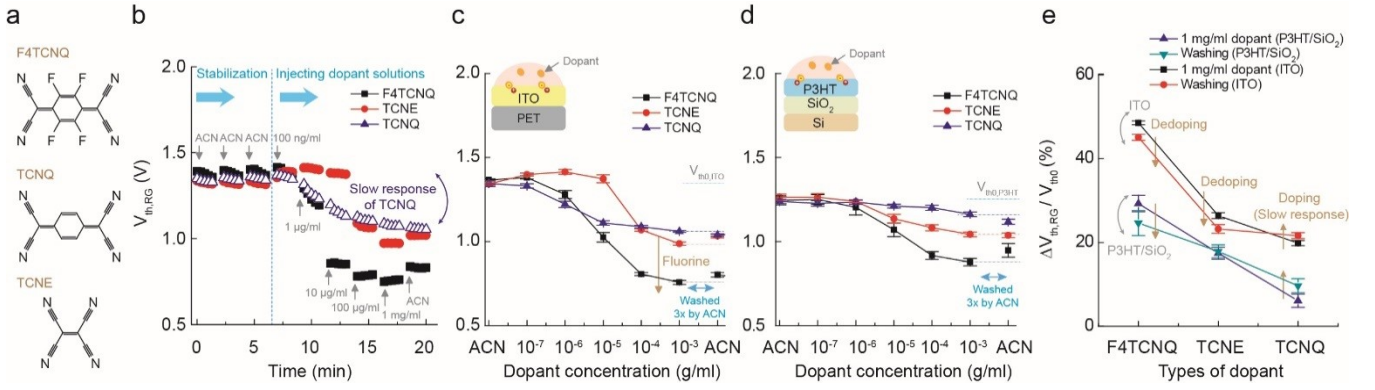


Figure 4. (a) Chemical structure of F4TCNQ, TCNQ, and TCNE. (b) Representative $V_{th,RG}$ response from neat ITO vs time for F4TCNQ, TCNE, and TCNQ solution concentrations. (c,d) $V_{th,RG}$ distributions over at least 6 samples vs. each dopant concentration measured by (c) ITO and (d) P3HT/SiO₂ RG, respectively. (e) Distribution of variation in $V_{th,RG}$ at 1 mg/ml F4TCNQ and neat ACN after washing with respect to each V_{th0} measured by the neat ITO and P3HT/SiO₂ RG over at least 6 samples.

ure 3f) and changes in Φ_{RG} given by F4TCNQ were a critical factor in making $V_{th,RG}$ shifts. $V_{th,RG}$ at 1 mg/ml F4TCNQ ($V_{th,1mg/ml}$) was slightly varied depending on the types of RG surface that offered different numbers of oxidizing sites of each RG. $V_{th,1mg/ml}$ of very thick drocast P3HT that was lower than that of spincoated P3HT (Figure 3e and Figure S4b) was almost comparable of that of ITO (Figure S4c).

Thus, p_d of P3HT on SiO₂ can be determined by assuming no loss in hole concentrations from any electron transfer and interface traps between SiO₂ and P3HT (Figure 3f). At equilibrium, the Fermi levels of undoped (E_F) and doped P3HT (E_{Fd}) are described with the equations of classic semiconductor physics as following:

$$E_F = -kT \ln\left(\frac{p_0}{N_v}\right) + E_{HOMO}$$

$$E_{Fd} = -kT \ln\left(\frac{p_d}{N_v}\right) + E_{HOMO}$$

where E_{HOMO} is energy level of the highest occupied molecular orbital, k is the Boltzmann constant, and T is temperature (K). N_v is defined as

$$N_v = 2 \left(\frac{2\pi m_p^* kT}{h^2} \right)^{3/2}$$

where m_p^* is effective mass of holes and h is Planck's constant. Therefore, ΔE_F ($E_{Fd} - E_F$) would be

$$\Delta E_F = kT \ln\left(\frac{p_0}{p_d}\right) \quad (2)$$

Also, ΔE_F is directly related to the change in work function of P3HT as shown in the inset of Figure 3g.

$$\Delta E_F = \Delta\phi_{P3HT} \quad (3)$$

Combining equation (1) above and (3) could establish following simple relation:

$$\Delta E_F = \Delta\phi_{P3HT} = \Delta\phi_{RG} = \Delta V_{th,RG} \quad (4)$$

By relating equations (2) and (4), we can arrive at the following equation to quantify the hole concentrations.

$$p_d = p_0 \exp\left(-\frac{\Delta V_{th,RG}}{kT}\right)$$

Based on p_0 of $2.4 \times 10^{17} / \text{cm}^3$ (Figure 2g) and average $\Delta V_{th,RG}$, p_d was calculated (Figure 3g). Also, p_d values calculated using UV-Vis NIR spectra (Figure S11) were compared in Figure 3g while the reliable values were only shown from F4TCNQ solution concentrations above 100 $\mu\text{g/ml}$ with distinguishable dopant peaks (Figure 1a). p_d values for heavily doped P3HT calculated both ways were comparable. μ_h of doped P3HT films was estimated based on p_d obtained by our model and $\sigma = e\mu_h p_d$. Highly doped P3HT showed the reduced mobility possibly from changed morphology. Each specific value in Figure 3g was tabulated in Table S1.

In addition, we measured $V_{th,RG}$ response of the other dopants such as TCNQ and TCNE with different reduction potentials (Figure 4a). $V_{th,RG}$ responses of ITO RG for TCNQ and TCNE vs time were compared in Figure 4b. While the doping effect of F4TCNQ and TCNE showed a step-shape $V_{th,RG}$ shift in our detection system, that of TCNQ was dragged over testing solution concentration ranges. This indicates that TCNQ slowly made surface dipoles. $V_{th,RG}$ at 1 mg/ml F4TCNQ and TCNE ($V_{th,1mg/ml}$) showed slightly increased V_{th0} after washing but $V_{th,1mg/ml}$ of TCNQ further lowered, resulting from delayed $V_{th,RG}$ response from slow reaction. By adding further washing steps (Figure S12), TCNQ was also washed off as was case of TCNE (Figure S12) and F4TCNQ (Figure S9). Washing effects were also observed through XPS in order to track elemental composition of the dopant on the surface (Figure S13). Compared to TCNQ, fluorine atoms shown in F4TCNQ with high electronegativity promoted faster and more electron transfer than TCNQ (Figure 4b and Figure 4c).

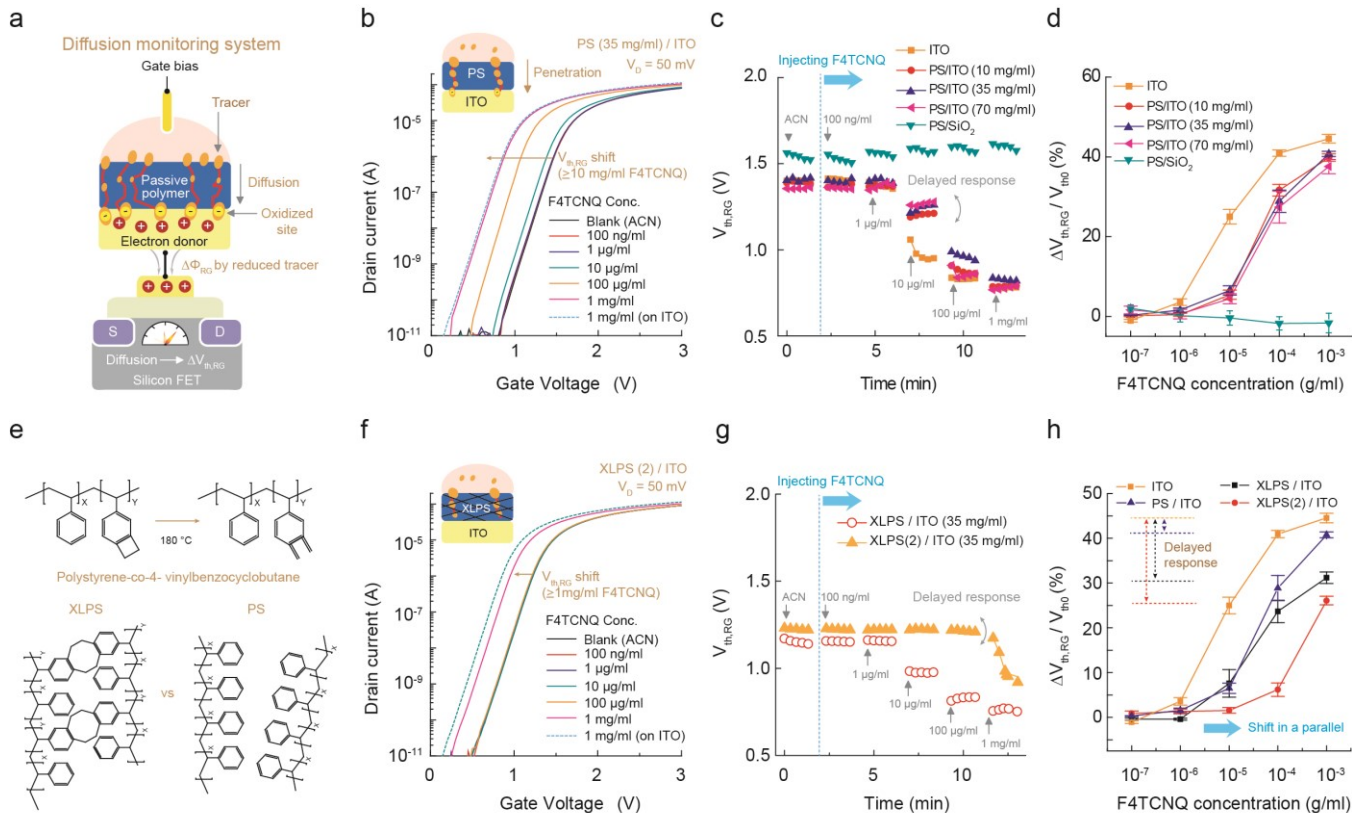


Figure 5. (a) Schematic image of diffusion monitoring system of small molecules through a passive polymer layer using RG FET system. (b) Representative response of transfer curves from PS/ITO RG for F4TCNQ solution concentrations. (c) Representative $V_{th, RG}$ response from the neat ITO, PS/SiO₂ and PS/ITO RG vs time for F4TCNQ solution concentrations. (d) Distributions of $V_{th, RG}$ variation with respect to V_{th0} from neat ITO, PS/SiO₂ and PS/ITO RGs over at least 8 samples. (e) Chemical polymer structure of PS and XLPS. (f) Representative response of transfer curves from XLPS (2) (indicating two depositions) on ITO RGs for F4TCNQ solution concentrations. (g) Representative $V_{th, RG}$ response from XLPS(2)/ITO and XLPS/ITO vs time for F4TCNQ solution concentrations. (h) Distributions of variation in $V_{th, RG}$ with respect to V_{th0} from the neat ITO, PS/ITO and XLPS/ITO RG over at least 8 samples.

Each dopant showed a similar trend in $V_{th, RG}$ shift with P3HT compared to those of ITO (Figure 4d). However, TCNE showed higher $V_{th, RG}$ response (≥ 1 μ g/ml) in P3HT film compared to that of ITO (≥ 10 μ g/ml), indicating better diffusion in P3HT because of its smaller size. Variations in V_{th} at 1 mg/ml solution concentration ($V_{th, 1mg/ml}$) and neat ACN after washing surface ($V_{th, wash}$) with respect to each V_{th0} were compared on both P3HT and ITO (Figure 4e). TCNE showed mostly no shift in $V_{th, wash}$ in P3HT but not in ITO. This could indicate that the smaller size of TCNE allowed a better fit in P3HT domains.

We now turn our attention to the additional application of the RG FET to monitor the diffusion of small molecules in a passive polymer such as PS. Briefly, ITO sensitive to F4TCNQ was used as sensing member for F4TCNQ that penetrated through a passive polymer on the ITO (Figure 5a). Representative transfer curves from PS/ITO RG are shown in Figure 5b. Although no interaction was observed between PS and F4TCNQ (Figure 2c), PS/ITO RG showed $V_{th, RG}$ response in terms of F4TCNQ concentrations (Figure 5c). This indicated that F4TCNQ diffused through PS and oxidized or bound to

the ITO surface. Despite the increased thicknesses of PS, the diffusion of F4TCNQ at high concentrations was observed with certain delayed response compared to that of neat ITO (Figure 5d).

Diffusion of F4TCNQ in cross-linked PS (XLPS) was measured. Cross-linking of PS polymer chains was made by using polystyrene-co-4-vinylbenzocyclobutane under high temperature of 180 °C (Figure 5e). Cross-linked polymer chain provided more rigid structures in the polymer layer against solution diffusion than normal PS. Representative transfer curves from double spin-coated XLPS RG were shown in Figure 5f. $V_{th, RG}$ response was mostly shown under high concentration of F4TCNQ solution of 1 mg/ml, indicating higher tolerance against the diffusion of F4TCNQ molecules. Single coated XLPS, however, showed higher $V_{th, RG}$ response comparable to that of normal PS (Figure 5g and 5h). This diffusion monitoring system is different from any conventional methods based on UV-Vis-NIR and PL spectroscopy that required interactions between host-materials and diffused molecules.

Conclusion

We developed a method to analyze doping effects and diffusion in polymers using a remote FET setup. Hole concentrations of P3HT doped via sequential doping methods were quantified by relating them to $V_{th,RG}$ shifts and work function changes in P3HT. In the detection mechanism, F4TCNQ occupied sites on electron donor surfaces by creating surface dipoles and the associated hole carriers imposed positive charges in P3HT, which was detected by an FET. As F4TCNQ fully covered the surfaces on electron donors, electronic potentials of electron donors were fully determined by F4TCNQ irrespective of types of materials. Almost all the bound F4TCNQ underwent integer charge transfer with those electron donors. Hole mobility of doped P3HT was derived from hole concentrations calculated from $V_{th,RG}$ shifts. We monitored physical diffusion of F4TCNQ in PS driven by concentration gradients using FET setup. This analysis provides a new electronic analysis tool to describe doping effects and diffusion in organic materials.

ASSOCIATED CONTENT

Supporting Information.

Detailed experimental, synthetic procedures, device fabrication, and the electronic characterization of the materials presented in this work.

AUTHOR INFORMATION

Corresponding Author

hekatz@jhu.edu

Author Contributions

Electrical measurements and device fabrication were carried out by H.-J. Jang and J. Wagner. Synthesis of XLPS was done by Q. Zhang. XPS and UV-Vis-NIR spectroscopy were measured by H.-J. Jang and J. Wagner. The manuscript was prepared by H.-J. Jang, H. Li, T. Mukhopadhyaya, and Howard E. Katz. All authors examined and commented on the manuscript. The project was guided by H. E. K.

Funding Sources

Principal support of this project was provided by the National Science Foundation, Division of Chemistry, grant number 1708245. The study of diffusion through PS and XL-PS was supported by the U.S. Department of Energy, Office of Science, Office of Basic Energy Sciences, under Award Number DEFG02-07ER46465. The development of the remote gate configuration was supported by the National Science Foundation, Division of Materials Research, grant number 1807292.

Notes

The authors declare no competing financial interest.

REFERENCES

1. Shirakawa, H.; Louis, E. J.; Macdiarmid, A. G.; Chiang, C. K.; Heeger, A. J., Synthesis of Electrically Conducting Organic Polymers - Halogen Derivatives of Polyacetylene, *(Ch)_x*. *J. Chem. Soc., Chem. Commun.*, **1977**, 578-580.
2. Lussem, B.; Keum, C. M.; Kasemann, D.; Naab, B.; Bao, Z. N.; Leo, K., Doped Organic Transistors. *Chem. Rev.* **2016**, *116*, 13714-13751.
3. Zhan, C. X.; Yu, G. Q.; Lu, Y.; Wang, L. Y.; Wujcik, E.; Wei, S. Y., Conductive polymer nanocomposites: a critical review of modern advanced devices. *J. Mater. Chem. C* **2017**, *5*, 1569-1585.
4. Zeglio, E.; Inganas, O., Active Materials for Organic Electrochemical Transistors. *Adv. Mater.* **2018**, *30*, 1800941-18.
5. Gould, C. M.; Bates, D. M.; Bozler, H. M.; Heeger, A. J.; Druy, M. A.; Macdiarmid, A. G., Electrical-Conductivity of Heavily Doped Polyacetylene at Ultralow Temperatures. *Phys. Rev. B* **1981**, *23*, 6820-6823.
6. Druy, M. A., The Role of the Counterion in the Reactivity of Conducting Polymers. *Synth. Met.* **1986**, *15*, 243-248.
7. Zhang, Y.; de Boer, B.; Blom, P. W. M., Controllable Molecular Doping and Charge Transport in Solution-Processed Polymer Semiconducting Layers. *Adv. Funct. Mater.* **2009**, *19*, 1901-1905.
8. Duong, D. T.; Wang, C. C.; Antono, E.; Toney, M. F.; Salleo, A., The chemical and structural origin of efficient p-type doping in P3HT. *Org. Electron.* **2013**, *14*, 1330-1336.
9. Saxman, A. M.; Liepins, R.; Aldissi, M., Polyacetylene: Its synthesis, doping and structure. *Prog. Polym. Sci.* **1985**, *11*, 57-89.
10. Zuo, G. Z.; Abdalla, H.; Kemerink, M., Impact of doping on the density of states and the mobility in organic semiconductors. *Phys. Rev. B* **2016**, *93*, 235203-8.
11. Jacobs, I. E.; Aasen, E. W.; Oliveira, J. L.; Fonseca, T. N.; Roehling, J. D.; Li, J.; Zhang, G. W.; Augustine, M. P.; Mascal, M.; Moule, A. J., Comparison of solution-mixed and sequentially processed P3HT:F4TCNQ films: effect of doping-induced aggregation on film morphology. *J. Mater. Chem. C* **2016**, *4*, 3454-3466.
12. Scholes, D. T.; Yee, P. Y.; Lindemuth, J. R.; Kang, H.; Onorato, J.; Ghosh, R.; Luscombe, C. K.; Spano, F. C.; Tolbert, S. H.; Schwartz, B. J., The Effects of Crystallinity on Charge Transport and the Structure of Sequentially Processed F₄TCNQ-Doped Conjugated Polymer Films. *Adv. Funct. Mater.* **2017**, *27*, 1702654-13.
13. Chew, A. R.; Ghosh, R.; Shang, Z. R.; Spano, F. C.; Salleo, A., Sequential Doping Reveals the Importance of Amorphous Chain Rigidity in Charge Transport of Semi-Crystalline Polymers. *J. Phys. Chem. Lett.* **2017**, *8*, 4974-4980.
14. Kang, S. D.; Snyder, G. J., Charge-transport model for conducting polymers. *Nat. Mater.* **2017**, *16*, 252-257.
15. Jones, M. L.; Huang, D. M.; Chakrabarti, B.; Groves, C., Relating Molecular Morphology to Charge Mobility in Semicrystalline Conjugated Polymers. *J. Phys. Chem. Lett. C* **2016**, *120*, 4240-4250.
16. Sirringhaus, H.; Brown, P. J.; Friend, R. H.; Nielsen, M. M.; Bechgaard, K.; Langeveld-Voss, B. M. W.; Spiering, A. J. H.; Janssen, R. A. J.; Meijer, E. W.; Herwig, P.; de Leeuw, D. M., Two-dimensional charge transport in self-organized, high-mobility conjugated polymers. *Nature* **1999**, *401*, 685-688.
17. Kline, R. J.; McGehee, M. D., Morphology and charge transport in conjugated polymer. *Polym. Rev.* **2006**, *46*, 27-45.
18. Pingel, P.; Schwarzl, R.; Neher, D., Effect of molecular p-doping on hole density and mobility in poly(3-hexylthiophene). *Appl. Phys. Lett.* **2012**, *100*, 143303-3.
19. Tietze, M. L.; Burtone, L.; Riede, M.; Lussem, B.; Leo, K., Fermi level shift and doping efficiency in p-doped small molecule organic semiconductors: A photoelectron spectroscopy and theoretical study. *Phys. Rev. B* **2012**, *86*, 035320-12.
20. Muller, L.; Rhim, S. Y.; Sivanesan, V.; Wang, D.; Hietzschold, S.; Reiser, P.; Mankel, E.; Beck, S.; Barlow, S.; Marder, S. R.; Pucci, A.; Kowalsky, W.; Lovrincic, R., Electric-Field-Controlled Dopant Distribution in Organic Semiconductors. *Adv. Mater.* **2017**, *29*, 1701466-7.
21. Li, J.; Rochester, C. W.; Jacobs, I. E.; Friedrich, S.; Stroeve, P.; Riede, M.; Moule, A. J., Measurement of Small Molecular Dopant F4TCNQ and C₆₀F₃₆ Diffusion in Organic Bilayer Architectures. *ACS Appl. Mater. Interfaces* **2015**, *7*, 28420-8.

22. Li, J.; Rochester, C. W.; Jacobs, I. E.; Aasen, E. W.; Friedrich, S.; Stroeve, P.; Moule, A. J., The effect of thermal annealing on dopant site choice in conjugated polymers. *Org. Electron.* **2016**, *33*, 23-31.
23. Chang, W. B.; Fang, H. Y.; Liu, J.; Evans, C. M.; Russ, B.; Popere, B. C.; Patel, S. N.; Chabinye, M. L.; Segalman, R. A., Electrochemical Effects in Thermoelectric Polymers. *ACS Macro. Lett.* **2016**, *5*, 455-459.
24. Tyagi, P.; Tuli, S.; Srivastava, R., Study of fluorescence quenching due to 2, 3, 5, 6-tetrafluoro-7, 7', 8, 8'-tetracyanoquinodimethane and its solid state diffusion analysis using photoluminescence spectroscopy. *J. Chem. Phys.* **2015**, *142*, 054707-8.
25. Wang, C. C.; Duong, D. T.; Vandewal, K.; Rivnay, J.; Salleo, A., Optical measurement of doping efficiency in poly(3-hexylthiophene) solutions and thin films. *Phys. Rev. B* **2015**, *91*, 085205-7.
26. Pingel, P.; Neher, D., Comprehensive picture of p-type doping of P3HT with the molecular acceptor F4TCNQ. *Phys. Rev. B* **2013**, *87*, 115209-9.
27. Panzram, E.; Baumgartel, H.; Roelfs, B.; Schroter, C.; Solomun, T., A Capacitance and Infrared Study of the Electrical Double-Layer Structure at Single-Crystal Gold Electrodes in Acetonitrile. *Chem. Phys.* **1995**, *99*, 827-837.
28. Iozzo, D. A. B.; Tong, M.; Wu, G.; Furlani, E. P., Numerical Analysis of Electric Double Layer Capacitors with Mesoporous Electrodes: Effects of Electrode and Electrolyte Properties. *J. Phys. Chem. C* **2015**, *119*, 25235-25242.
29. Pullano, S. A.; Critello, C. D.; Mahub, I.; Tasneem, N. T.; Shamsir, S.; Islam, S. K.; Greco, M.; Fiorillo, A. S., EGFET-Based Sensors for Bioanalytical Applications: A Review. *Sensors* **2018**, *18*, 4042-24.
30. Chang, J. F.; Sun, B. Q.; Breiby, D. W.; Nielsen, M. M.; Solling, T. I.; Giles, M.; McCulloch, I.; Siringhaus, H., Enhanced mobility of poly(3-hexylthiophene) transistors by spin-coating from high-boiling-point solvents. *Chem. Mater.* **2004**, *16*, 4772-4776.
31. Schneider, M.; Wagenfahl, A.; Deibel, C.; Dyakonov, V.; Scholl, A.; Reinert, F., Band bending at the P3HT/ITO interface studied by photoelectron spectroscopy. *Org. Electron.* **2014**, *15*, 1552-1556.
32. Lue, C. E.; Wang, I. S.; Huang, C. H.; Shiao, Y. T.; Wang, H. C.; Yang, C. M.; Hsu, S. H.; Chang, C. Y.; Wang, W.; Lai, C. S., pH sensing reliability of flexible ITO/PET electrodes on EGFETs prepared by a roll-to-roll process. *Microelectron. Reliab.* **2012**, *52*, 1651-1654.
33. David E. Yates, S. L., Thomas W. Healy, Site-Binding Model of the Electrical Double Layer at the Oxide/Water Interface. *J. Chem. Soc., Faraday Trans. 1*, **1973**, *70*, 1807-1818

Table of contents entry

